

## REVIEW

View Article Online  
View Journal | View IssueCite this: *Mater. Chem. Front.*,  
2024, 8, 769

# Acceptor–donor–acceptor based thermally activated delayed fluorescent materials: structure–property insights and electroluminescence performances

Keshavananda Prabhu C P, <sup>a</sup> Kenkera Rayappa Naveen <sup>†\*b</sup> and Jaehyun Hur <sup>\*a</sup>

Organic light-emitting diodes (OLEDs) have transformed the display and lighting industries with their high electroluminescence, flexibility, and tunable colors. After fluorescent and phosphorescent materials, thermally activated delayed fluorescence (TADF) materials have emerged as low-cost emitters to enhance OLED performances efficiently by harvesting both singlet and triplet excitons and converting them into light emission. Among the developed conventional TADF materials, there has been intense research with different classes, such as D–A, D–A–D, and D– $\pi$ –A. However, recently, a new class states that Acceptor–Donor–Acceptor (ADA) molecules, known for their efficient charge-transfer nature, have exhibited significant potential as prominent TADF emitters for high electroluminescent OLEDs. However, there is no clear understanding of their structural insights for ADA-based TADF materials. So there needs to be a comprehensive understanding of the aspect of the molecular design and structure–property relationship. To fill this gap, we presented a comprehensive, in-depth review of ADA-based TADF materials, encompassing their molecular design principles, photo-physical mechanisms, device architectures, and current challenges faced in this era. Finally, the future perspective of this class of materials in forthcoming highly efficient OLED displays is also discussed.

Received 16th October 2023,  
Accepted 3rd November 2023

DOI: 10.1039/d3qm01125a

rsc.li/frontiers-materials

## 1. Introduction

Organic light-emitting diode (OLED) technology has been extensively applied in high-end solid-state lighting and flat-panel displays due to its superior advantages of low driving voltage, flexibility, fast response, and wide viewing angle.<sup>1–5</sup> According to the spin-statistics rules, electro generated excitons have a ratio of 1 : 3 with 25% singlet and 75% triplet excitons. Conventional fluorescent materials (first generation) with high photoluminescence quantum yields (PLQYs) can only utilize singlet excitons, while the energies of triplet excitons have deviated *via* nonradiative transition processes.<sup>6–11</sup> To realize full exciton utilization, phosphorescence and thermally activated delayed fluorescence (TADF) emitters have been proposed as second and third-generation OLED materials.<sup>6–11</sup> All the three generations with an emission/exciton mechanism and basic

OLED device architecture are illustrated in Fig. 1. Phosphorescence emitters can utilize 100% triplet excitons due to the strong spin–orbit coupling (SOC) induced by metal atoms (*e.g.*, platinum (Pt) and iridium (Ir)), which can help to enhance the triplet radiation rate with the help of intersystem crossing (ISC).<sup>8,12</sup> Although phosphorescence-based OLEDs are now the leading commercial OLED technologies, they have several obvious drawbacks, such as high costs and toxicity due to metal atoms.<sup>8,13</sup>

TADF-based OLEDs are an alternative tool with potential 100% internal quantum efficiencies (IQEs) utilizing 100% singlet excitons and have attracted considerable attention from the past decade.<sup>9,14–25</sup> Furthermore, they are not so expensive to make, which is keen for future OLED applications. The key to obtain efficient TADF materials is to achieve a small singlet and triplet excited state gap ( $\Delta E_{ST}$ ).<sup>16,26–28</sup> Based on the exchange energy, it is understood that the small  $\Delta E_{ST}$  can be achieved by spatially separated highly occupied molecular orbital (HOMO) and lowest unoccupied molecular orbital (LUMO) distributions.<sup>17,27,29–32</sup> Suppose if  $\Delta E_{ST}$  is small for the designed molecule, then the reverse intersystem crossing (RISC) also will be effective and can show prominent TADF characteristics.<sup>33,34</sup> Initially, Donor–Acceptor (D–A) based TADF materials were designed for high

<sup>a</sup> Department of Chemical and Biological Engineering, Gachon University, Seongnam-si 13120, Gyeonggi-do, Korea. E-mail: jhhur@gachon.ac.kr

<sup>b</sup> Institut für Anorganische Chemie and Institute for Sustainable Chemistry & Catalysis with Boron, Julius-Maximilians-Universität Würzburg, Am Hubland, 97074 Würzburg, Germany. E-mail: naveen.kr012@gmail.com

† These authors contributed equally.

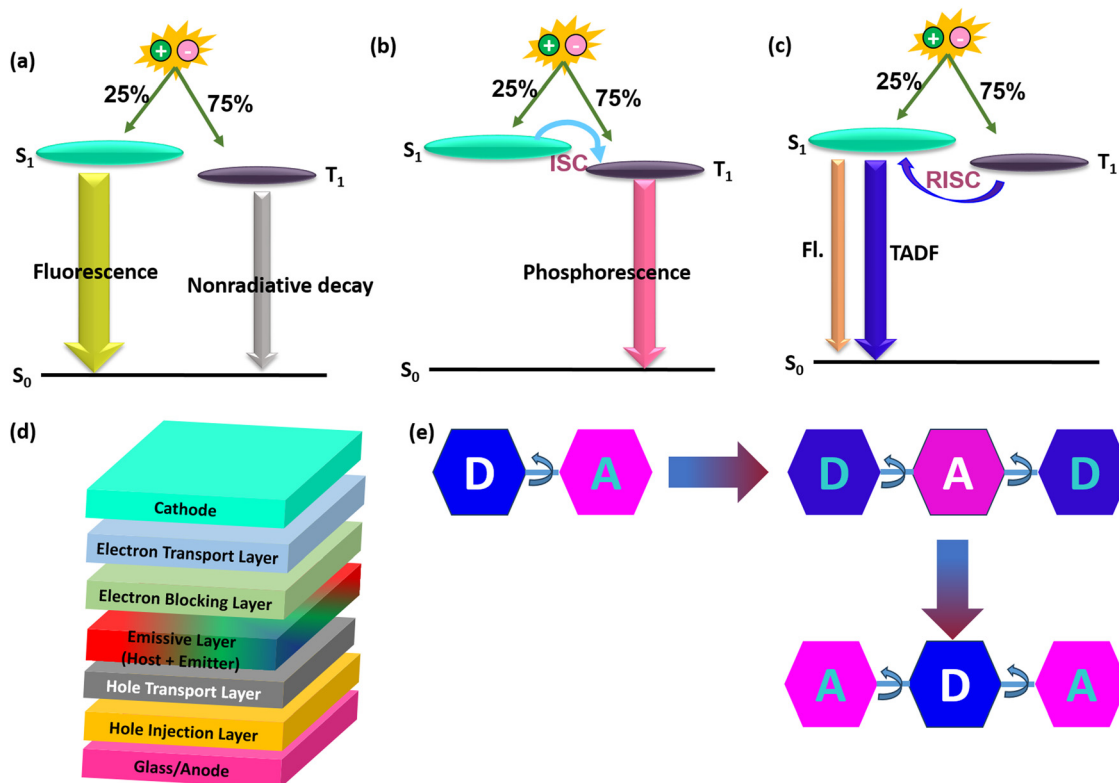


Fig. 1 Exciton pathways for (a) fluorescence, (b) phosphorescence, and (c) thermally activated delayed fluorescence; (d) basic organic light emitting diode architecture; (e) main TADF materials revolutionary pathways.

electroluminescence OLED performances. These materials were mostly manifested by the well separated HOMO and LUMO on D and A moieties.<sup>17,18,35–38</sup> Usually when the molecule excites, D can transfer the electron to A, resulting in the formation of a charge transfer (CT) excited state for TADF to be active. Based on D–A based designs, the TADF materials showed a high external quantum efficiency (EQE) of over 30% without utilizing any sensitizers in the OLED fabrication.<sup>35,39,40</sup> The state of the art materials among them are TDBA-DI for blue,<sup>41</sup> DACT-II for green,<sup>34</sup> and PQ3 for red,<sup>42</sup> respectively. Later on, to extend the TADF materials, several types were developed enormously, such as D– $\pi$ –A,<sup>43</sup> D–A–D,<sup>44</sup> and D–A–A,<sup>45</sup> respectively.<sup>46</sup> Among the developed TADF materials, some of the most commonly used acceptors are triazine, pyridine, pyrimidine, and naphthalimide, and donors are carbazole, acridine, phenoxazine, phenothiazine, indolocarbazole, and spiro based donors.<sup>47</sup> On the other hand, boron-based acceptor inserted materials were also developed mainly for blue OLEDs.<sup>48–53</sup> Even though there have been many developments with the abovementioned types, they showed limited horizontal dipole orientation for light emission in OLEDs.<sup>54–56</sup> Usually, elongating molecular conjugation along the direction of the transition dipole moment and expanding the molecular plane where the transition dipole moment lies are the main two strategies to improve the horizontal dipole orientation values. This will help to improve the outcoupling efficiency of the devices, and promote the device external quantum efficiencies.

So later on, Acceptor–Donor–Acceptor (A–D–A) based TADF materials were developed to surpass the dipole orientation ratios for OLEDs.<sup>57</sup>

As an initial approach for A–D–A TADF emitters, pyrimidine as an acceptor and indolocarbazole as a donor in A–D–A based TADF materials were developed. They were showing sky blue emissions with a limited EQE of  $\sim 12\%$ .<sup>57</sup> Later, there have been vast developments reported recently utilizing the triazine and boron based acceptor moieties. On the other hand, there is a sub-class of TADF materials named multi-resonance TADF (MR-TADF), also developed for pure color enhancements.<sup>58–63</sup> These materials manifested narrowband emission with a full width at half maximum (FWHM) of  $< 40$  nm due to the suppressed vibronic transitions and advantageous short-range charge transfer (SRCT) characteristics.<sup>59,64–81</sup> Recently, based on the boron acceptors in A–D–A based design, Kwon *et al.* achieved the highly stable red TADF-OLEDs with a horizontal dipole orientation of over 0.74 and a maximum EQE of 30.3% with extremely low roll-off characteristics.<sup>82</sup> Later, several A–D–A based TADF materials were developed for wide color gamut regions with excellent EQEs over 30% with good TADF properties, high PLQYs, and high molecular orientations. Still, achieving a high color purity and horizontal dipole orientation remains challenging. To the best of our knowledge, no review emphasizes A–D–A based TADF materials. So in this review, we describe the recent advancements in A–D–A based TADF emitters (including MR-TADF) based on their molecular design strategy, photophysical

characterization, and detailed electroluminescence performances. We divided the sections based on the donor types such as carbazole, indolocarbazole, phenazine, and spiro based donors in A–D–A based TADF materials. Furthermore, this review explains the advantages and disadvantages of conventional A–D–A TADF emitters. Finally, the future perspectives of this class of materials in forthcoming OLED displays are also discussed.

## 2. Results and discussion

### 2.1. Carbazole and indolocarbazole based donors in A–D–A type TADF Materials

Initially, Adachi *et al.* successfully demonstrated two efficient blue-green thermally activated delayed fluorescence (TADF) compounds by incorporating a dimeric phenyl carbazole backbone with four cyano substituents on the phenyl rings (Fig. 2). The researchers compared the properties of the 2,6-dicyano-substituted derivative (**26IPNDCz**) with the 3,5-dicyano-substituted derivative (**35IPNDCz**), which acts as an acceptor (A) with 3,3'-bicarbazolyl as the donor (D).<sup>83</sup> By varying the position of the cyano groups on the phenyl rings, the twisting

angle between the donor and acceptor moieties could be adjusted. The authors observed that ortho-substitution resulted in a larger twisting angle due to steric hindrance, leading to a more efficient separation of the HOMO and LUMO. Both compounds exhibited the TADF phenomenon. However, the one with the larger twisting angle (**26IPNDCz**) showed a smaller  $\Delta E_{ST}$  and shorter TADF lifetime (Table 1). The fabricated OLEDs based on **26IPNDCz** achieved an EQE of 10% with reduced efficiency roll-off, making it a promising candidate for efficient TADF-based OLEDs (Table 2). These findings shed light on the importance of A–D–A based molecular design and structural modifications to enhance the TADF properties and OLED performance of such bipolar compounds. This study embarks valuable insights into developing efficient blue-green TADF emitters. It provides a basis for optimizing the performance of TADF-based OLEDs through careful structural adjustments and design strategies.

Colman *et al.* introduced a groundbreaking difunctionalized indolocarbazole-based emitter, **ICzTRZ**, representing a significant milestone in OLED technology.<sup>84</sup> The design is based on utilizing the two diphenyl triazine-based acceptors with indolocarbazole as the donor. One remarkable characteristic of this

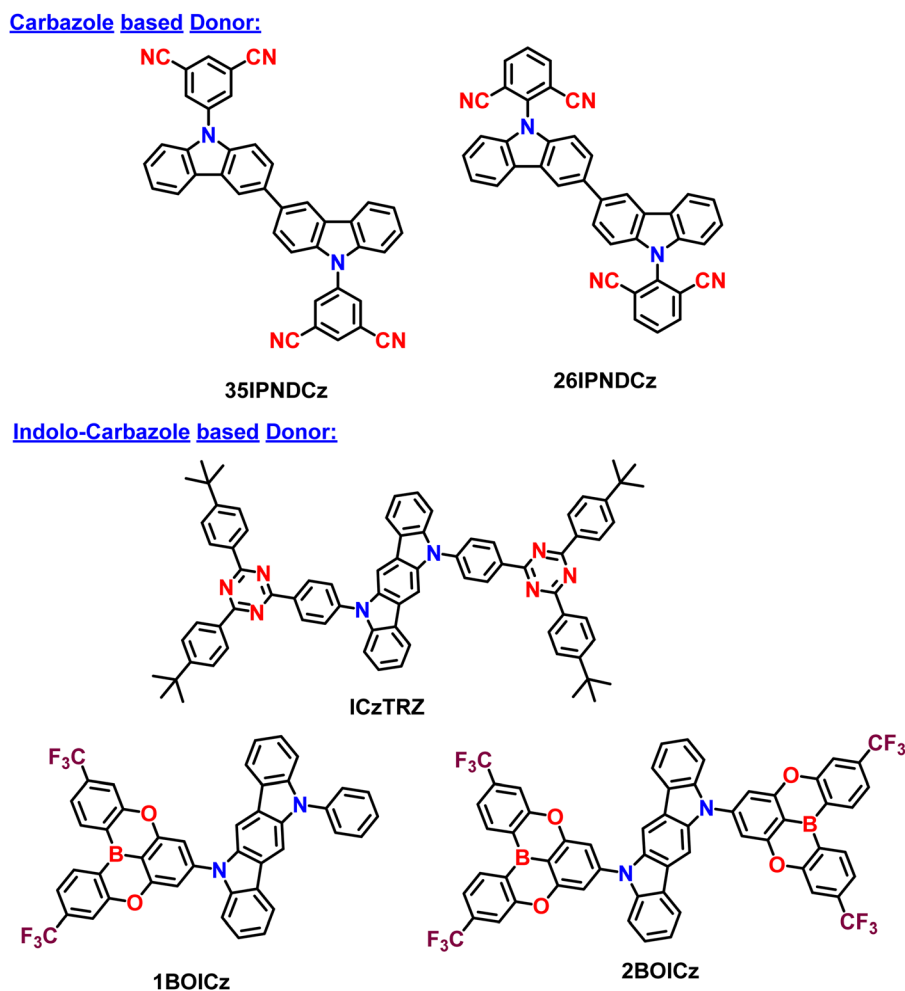


Fig. 2 Chemical structures of A–D–A type TADF materials based on carbazole and indolocarbazole based donors.

Table 1 Detailed photophysical properties of A–D–A based TADF materials

| Emitter               | PL <sub>max</sub> (nm) | PLQY [%] | HOMO [eV] | LUMO [eV] | S <sub>1</sub> [eV] | T <sub>1</sub> [eV] | ΔE <sub>ST</sub> [eV] | τ <sub>p</sub> (ns) | τ <sub>d</sub> (μs) | RISC (×10 <sup>5</sup> s <sup>-1</sup> ) | Ref. |
|-----------------------|------------------------|----------|-----------|-----------|---------------------|---------------------|-----------------------|---------------------|---------------------|------------------------------------------|------|
| 35IPNDCz              | 470                    | 50       | —         | —         | —                   | —                   | 0.14                  | 24                  | 145                 | —                                        | 83   |
| 26IPNDCz              | 488                    | 72       | —         | —         | —                   | —                   | 0.06                  | 28                  | 9.2                 | —                                        |      |
| ICzTRZ                | 462                    | 56       | -5.66     | -3.17     | 2.94                | 2.62                | 0.32                  | 9                   | 229.2               | —                                        | 84   |
| ICzTRZ (5 wt% mCBP)   | 479                    | 59       | —         | —         | 2.85                | 2.62                | 0.23                  | 8.7                 | 121.1               | —                                        |      |
| ICzTRZ (10 wt% PMMA)  | 470                    | 28       | —         | —         | 2.75                | 2.64                | 0.11                  | 11.5                | 252.8               | —                                        |      |
| 1TICz                 | 495                    | 90       | -5.56     | -2.76     | 2.78                | 2.61                | 0.17                  | 11                  | 989                 | 1.1                                      | 85   |
| 1BOICz                | 534                    | 90       | -5.89     | -3.26     | 2.65                | 2.60                | 0.05                  | 20                  | 968                 | 11.2                                     |      |
| 2BOICz                | 528                    | 89       | -6.02     | -3.38     | 2.69                | 2.63                | 0.06                  | 16                  | 884                 | 11.8                                     |      |
| DHPZ-2BI              | 537                    | 68       | -5.30     | -2.85     | —                   | —                   | 0.19                  | 4                   | 50                  | —                                        | 87   |
| DHPZ-2BN              | 541                    | 35       | -5.34     | -3.02     | —                   | —                   | 0.10                  | 7                   | 7                   | —                                        |      |
| DHPZ-2BTZ             | 577                    | 33       | -5.30     | -2.92     | —                   | —                   | ~0                    | 12                  | 1                   | —                                        |      |
| DHPZ-2TRZ             | 598                    | 7        | -5.28     | -3.18     | —                   | —                   | —                     | 6                   | 0.1                 | —                                        |      |
| PzTDBA (5%)           | 599                    | 100      | -4.94     | -2.71     | 2.21                | 2.15                | 0.06                  | 44.6                | 2.6                 | 11.9                                     | 82   |
| PzTDBA (10%)          | —                      | 82       | —         | —         | —                   | —                   | —                     | 38.8                | 2.1                 | 9.5                                      |      |
| PzTDBA (20%)          | —                      | 77       | —         | —         | —                   | —                   | —                     | 42.2                | 1.9                 | 8.4                                      |      |
| PzDBA (5%)            | 610                    | 85       | -4.98     | -2.80     | 2.16                | 2.11                | 0.05                  | 32.6                | 2.0                 | 8.4                                      |      |
| PzDBA (10%)           | —                      | 68       | —         | —         | —                   | —                   | —                     | 42.3                | 1.8                 | 9.5                                      |      |
| PzDBA (20%)           | —                      | 41       | —         | —         | —                   | —                   | —                     | 40.6                | 40.6                | 1.9                                      |      |
| QxPz                  | 598                    | 62       | -5.29     | -2.89     | —                   | —                   | —                     | 20.3                | 1.2                 | 0.11                                     | 88   |
| DMQxPz                | 576                    | 85       | -5.28     | -2.82     | —                   | —                   | —                     | 19.6                | 1.2                 | 0.12                                     |      |
| DPQxPz                | 613                    | 66       | -5.29     | -2.98     | —                   | —                   | —                     | 15.2                | 2.2                 | 0.08                                     |      |
| 2BNCz-PZ              | 586                    | 96       | -4.70     | -2.50     | 2.30                | 2.26                | 0.04                  | 32.9                | 1.5                 | 18                                       | 90   |
| 2BNtCz-PZ             | 586                    | 93       | -4.60     | -2.50     | 2.45                | 2.43                | 0.02                  | 32.8                | 1.4                 | 23                                       |      |
| 2PXZ-2TRZ             | 509                    | 94       | -5.31     | -3.02     | 2.68                | 2.67                | 0.01                  | 108                 | 5.3                 | 6.0                                      | 91   |
| DBA-SAB               | 472                    | 87       | -5.60     | -2.5      | —                   | —                   | 0.07                  | 45.1                | 1                   | 19.0                                     | 17   |
| TRZ-SBA-NAI           | 577                    | 87       | -5.42     | -3.24     | 2.45                | 2.29                | 0.16                  | 16.7                | 398                 | —                                        | 93   |
| TPA-2PPI              | 437                    | 85       | —         | —         | —                   | —                   | —                     | —                   | —                   | —                                        | 94   |
| PPI-2BI               | 440                    | 82       | -5.54     | -2.60     | —                   | —                   | —                     | —                   | —                   | —                                        | 95   |
| 2CzOXD                | 449                    | 9        | -5.65     | -2.30     | 3.09                | 2.70                | 0.39                  | —                   | —                   | —                                        | 96   |
| 4CzOXD                | 443                    | 6        | -5.51     | -2.25     | 3.11                | 2.97                | 0.14                  | —                   | —                   | —                                        |      |
| 4CzDOXD               | 581                    | 92       | -5.66     | -2.96     | 2.54                | 2.52                | 0.02                  | 23.2                | 1.4                 | 0.19                                     |      |
| 4tCzDOXD              | 603                    | 71       | -5.53     | -2.72     | 2.58                | 2.56                | 0.02                  | 18.9                | 1.0                 | 0.29                                     |      |
| DIDOBNA-N (sol)       | 426                    | 73       | -5.49     | -1.51     | 3.08                | 2.86                | 0.22                  | 3.07                | —                   | —                                        | 97   |
| DIDOBNA-N (film)      | 444                    | 81       | —         | —         | 3.12                | 2.89                | 0.23                  | 6.83                | 13.7                | 0.31                                     |      |
| MesB-DIDOBNA-N (sol)  | 399                    | 33       | -5.60     | -1.46     | 3.17                | 2.93                | 0.24                  | 2.63                | —                   | —                                        |      |
| MesB-DIDOBNA-N (film) | 402                    | 75       | —         | —         | 3.18                | 2.94                | 0.24                  | 5.09                | 95.9                | 0.09                                     |      |
| TPA-QX                | 535                    | 44       | -5.25     | -3.00     | —                   | —                   | 0.38                  | 30.2                | —                   | —                                        | 98   |
| PXZ-QX                | 573                    | 32       | -5.11     | -3.01     | —                   | —                   | 0.24                  | 62.3                | —                   | —                                        |      |
| DPXZ-QX               | 582                    | 74       | -5.10     | -2.95     | —                   | —                   | 0.09                  | 91.0                | 26.9                | 1.86                                     |      |
| DPXZ-DFQX             | 595                    | 71       | -5.11     | -3.02     | —                   | —                   | 0.01                  | 144.1               | 6.8                 | 4.33                                     |      |
| DPXZ-2QX              | 594                    | 87       | -5.09     | -2.92     | —                   | —                   | 0.02                  | 151.8               | 8.7                 | 8.21                                     |      |
| DPXZ-2DFQX            | 599                    | 91       | -5.13     | -3.02     | —                   | —                   | -0.05                 | 155.9               | 4.9                 | 4.64                                     |      |

material is its nearly complete horizontal orientation when incorporated into three different host matrices. This unique feature dramatically enhances the light out-coupling efficiency in OLEDs, making it a highly desirable choice for optoelectronic applications. The emitter's exceptional orientation behavior can be attributed to its elongated, stick-like structure. Additionally, the emitter **ICzTRZ** exhibits a high PLQY, further contributing to its outstanding performance in OLED devices. However, achieving maximum EQE in OLEDs also relies on enhancing light out-coupling efficiency. As a result, The **ICzTRZ** manifested sky-blue electroluminescence with an emission wavelength ( $\lambda_{\text{EL}}$ ) of 483 nm and CIE coordinates of 0.17 and 0.32. The fabricated OLED device obtained an impressive EQE<sub>max</sub> of 22.1% with a maximum luminance of 7800 cd m<sup>-2</sup>. Such high values are due to the high horizontal dipole orientation factor (~91%) of the A–D–A type TADF scaffold. This pioneering work opens up new possibilities for designing efficient and high-performance OLEDs based on stable acceptors in A–D–A type TADF designs, pushing the boundaries of display and lighting technologies.

Very recently, Duan *et al.* have recently extended the A–D–A type TADF materials, similar to **ICzTRZ**. They developed new materials by utilizing the CF<sub>3</sub>-embedded fully fused oxygen bridged acceptors, 5,9-dioxa-13*b*-boranaphtho[3,2,1-*de*]anthracene (**DOBNA**) and the same indolocarbazole (ICz) as a donor (Fig. 3).<sup>85</sup> Owing to its slight MR-type character,<sup>86</sup> **DOBNA** exhibits an elongated rigid structure with high TADF properties when it is attached to a sterically uncrowded indolocarbazole (ICz) donor. They manifested hybrid electronic excitations characterized by a main donor-to-acceptor long-range (LR) and an auxiliary bridge-phenyl short-range (SR) charge transfer. Such excitations allow us to get the small ΔE<sub>ST</sub> and a large oscillator strength (*f*). Moreover, due to the dual CT states, the developed emitter (**2BOICz**) doubled the *f* value without affecting the ΔE<sub>ST</sub> compared to a simple D–A based TADF emitter (**1BOICz**). Furthermore, the **2BOICz** showed a high radiative decay rate, even higher than the ISC rate. On the other hand, due to the short exciton delayed lifetime of ~0.88 μs, the RISC rate value is > 10<sup>6</sup> s<sup>-1</sup>. Furthermore, as the key point, **2BOICz** has tremendously manifested a high horizontal emitting dipole

Table 2 Detailed Electroluminescence performances of the A–D–A based TADF–OLEDs

| Emitter           | Host       | $\theta_{\parallel}$ | CE (cd/A) | EQE (%) | EL <sub>max</sub> [nm] | FWHM [nm] | CIE (x,y)    | Ref. |
|-------------------|------------|----------------------|-----------|---------|------------------------|-----------|--------------|------|
| 35IPNDCz          | DPEPO      | —                    | —         | 9.2     | 487                    | —         | —            | 83   |
| 26IPNDCz          | DPEPO      | —                    | —         | 9.6     | 501                    | —         | —            |      |
| ICzTRZ            | mCBP       | 0.91                 | —         | 22.10   | 483                    | —         | (0.17; 0.32) | 84   |
| 1TICz             | mCPBC      | 0.84                 | —         | 26.10   | 504                    | 100       | (0.25; 0.50) | 85   |
| 1BOICz            | mCPBC      | 0.85                 | —         | 34.60   | 534                    | 101       | (0.38; 0.57) |      |
| 2BOICz            | mCPBC      | 0.91                 | —         | 40.40   | 528                    | 91        | (0.38; 0.55) |      |
| DHPZ-2BI          | mCBP       | —                    | —         | 12      | 542                    | —         | —            | 87   |
| DHPZ-2BN          | mCBP       | —                    | —         | 6       | 546                    | —         | —            |      |
| DHPZ-2BTZ         | mCBP       | —                    | —         | 5       | 601                    | —         | —            |      |
| DHPZ-2TRZ         | mCBP       | —                    | —         | 1       | 617                    | —         | —            |      |
| PzTDBA (5 wt%)    | Mixed host | 0.79                 | 68.70     | 30.30   | 576                    | —         | (0.49; 0.50) | 82   |
| PzTDBA (10 wt%)   | Mixed host | —                    | 60.60     | 28.80   | 581                    | —         | (0.51; 0.48) |      |
| PzTDBA (20 wt%)   | Mixed host | —                    | 50.80     | 26.60   | 588                    | —         | (0.53; 0.46) |      |
| PzDBA (5 wt%)     | Mixed host | 0.74                 | 35.70     | 21.80   | 595                    | —         | (0.55; 0.45) |      |
| PzDBA (10 wt%)    | Mixed host | —                    | 25.90     | 18.80   | 604                    | —         | (0.57; 0.43) |      |
| PzDBA (20 wt%)    | Mixed host | —                    | 15.60     | 13.40   | 613                    | —         | (0.60; 0.40) |      |
| QxPz              | CBP        | —                    | 26.80     | 13.40   | 598                    | —         | (0.48; 0.50) | 88   |
| DMQxPz            | CBP        | —                    | 54.00     | 19.90   | 576                    | —         | (0.54; 0.45) |      |
| DPQxPz            | CBP        | —                    | 25.60     | 15.40   | 612                    | —         | (0.56; 0.43) |      |
| 2BNCz-PZ          | mCBP       | 0.85                 | 56.3      | 29.0    | 600                    | —         | (0.55; 0.44) | 90   |
| 2BNtCz-PZ         | mCBP       | 0.91                 | 61.6      | 31.0    | 602                    | —         | (0.56; 0.43) |      |
| 2PXZ-2TRZ         | PPF        | —                    | 65.0      | 27.1    | 508                    | —         | (0.26; 0.54) | 91   |
| DBA-SAB           | DPEPO      | 0.89                 | 43.80     | 25.70   | 472                    | —         | (0.14; 0.21) | 17   |
| TRZ-SBA-NAI       | mCPCN      | 0.88                 | 71.00     | 31.70   | 593                    | —         | (0.55; 0.45) | 93   |
| TPA-2PPI          | —          | —                    | 4.76      | 4.91    | 452                    | —         | (0.15; 0.11) | 94   |
| TPA-PPI           | —          | —                    | 5.66      | 5.02    | 434                    | —         | (0.15; 0.11) |      |
| PPI-2BI (M)       | CBP        | —                    | 4.98      | 4.63    | 452                    | —         | (0.16; 0.12) | 95   |
| PPI-2BI (B)       | CBP        | —                    | 4.42      | 3.81    | 444                    | —         | (0.16; 0.12) |      |
| PPI-2BI (D)       | CBP        | —                    | 1.78      | 4.12    | 432                    | —         | (0.15; 0.05) |      |
| 4CzDOXD           | CBP        | —                    | 62.30     | 19.40   | 520                    | —         | (0.30; 0.57) | 96   |
| 4tCzDOXD          | CBP        | —                    | 68.60     | 20.80   | 530                    | —         | (0.33; 0.57) |      |
| 4CzDOXD           | o-CzOXD    | —                    | 62.60     | 20.30   | —                      | —         | (0.29; 0.55) |      |
| 4tCzDOXD          | o-CzOXD    | —                    | 74.50     | 22.60   | —                      | —         | (0.34; 0.57) |      |
| DIDOBNA-N         | TSPO1      | —                    | —         | 15.20   | —                      | 70        | (0.15; 0.07) | 97   |
| MesB-DIDOBNA-N    | TSPO1      | —                    | —         | 9.30    | —                      | 22        | (0.16; 0.04) |      |
| MesB-DIDOBNA-N    | CzSi:TSPO1 | —                    | —         | 16.20   | —                      | 21        | (0.17; 0.05) |      |
| DPXZ-QX (3 wt%)   | mCBP       | —                    | 48.02     | 19.40   | 594                    | —         | (0.48; 0.43) | 98   |
| DPXZ-QX (6 wt%)   | mCBP       | —                    | 48.60     | 20.56   | 597                    | —         | (0.52; 0.44) |      |
| DPXZ-QX (12 wt%)  | mCBP       | —                    | 37.56     | 18.86   | 599                    | —         | (0.56; 0.43) |      |
| DPXZ-2QX (3 wt%)  | mCBP       | —                    | 37.75     | 19.95   | 605                    | —         | (0.56; 0.42) |      |
| DPXZ-2QX (6 wt%)  | mCBP       | —                    | 38.59     | 23.16   | 609                    | —         | (0.59; 0.41) |      |
| DPXZ-2QX (12 wt%) | mCBP       | —                    | 30.88     | 21.14   | 616                    | —         | (0.60; 0.39) |      |

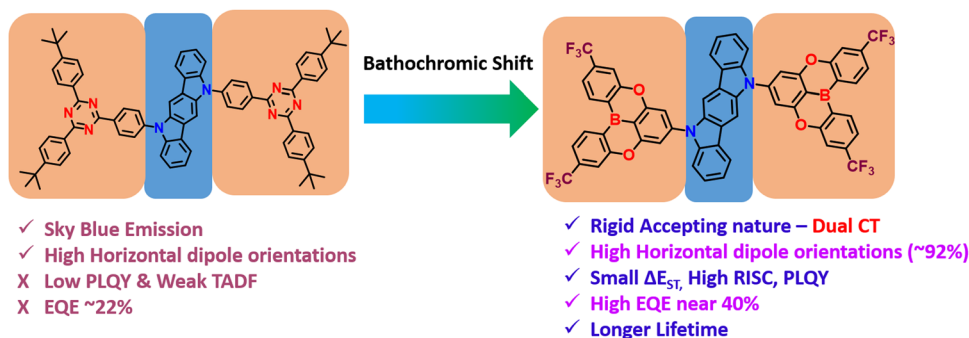


Fig. 3 Merits of the rigid acceptors in A–D–A type TADF designs.

orientation of 91.6% compared to **1BOICz** (85.5%). This horizontal emitting dipole orientation value is the sound record for all the developed A–D–A based TADF materials due to the large quasi-planar structural motifs. Furthermore, this sizeable molecular planarity should render the molecular orientation

perfectly parallel to the base plane during evaporation. Then the fabricated OLEDs based on **2BOICz** with **mCPBC** as a host exhibited a high EQE of 40.4% with alleviated EQE roll-off characteristics and extended operational lifetimes in the green region. Such high EQE values are highly attributed due to the



high planarity of the molecules in A–D–A combinations. Considering the heavy atoms such as sulfur and selenium in this A–D–A based design, RISC can be further boosted with the support of enhanced SOC values and dual CT characteristics.

## 2.2. Phenazine as a donor in A–D–A based TADF materials

Even though carbazole-based A–D–A based TADF materials showed a high EQE of over 30% in OLEDs, they are limited in blue and green regions only due to their weak donating ability.

So, to enhance and elaborate the wide color gamut regions further, the 5,10-dihydrophenazine as donor based materials were also developed for A–D–A based TADF based molecular designs. In 2015, Adachi *et al.* developed a series of TADF materials by utilizing the 5,10-dihydrophenazine as an electron donor and various electron acceptor scaffolds. The developed materials based on the A–D–A type are named **DHPZ-2BI**, **DHPZ-2BN**, **DHPZ-2BTZ**, and **DHPZ-2TRZ**, respectively, by varying the acceptor units (Fig. 4).<sup>87</sup> These materials manifested

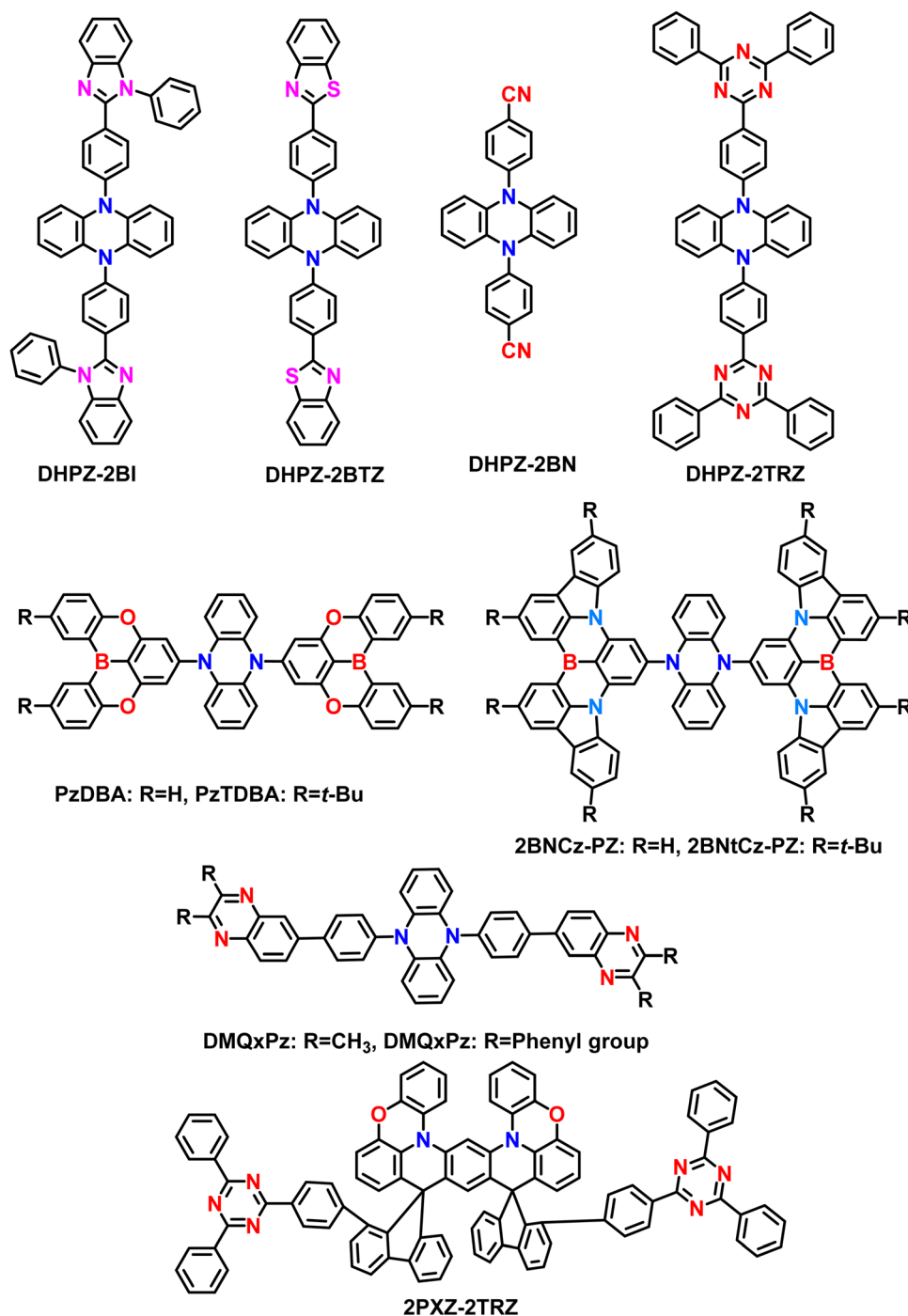


Fig. 4 Chemical structures discussed with phenazine as a donor in A–D–A type TADF materials.

small  $\Delta E_{ST}$  ranging from approximately 0 to 0.19 eV, with an emission color from green to orange regions. The excitons delayed fluorescence lifetimes of these materials are varied from 0.1 to 50  $\mu$ s. Among the developed materials, **DHPZ-2BI** showed an improved PLQY of around 67% compared to others. These high PLQY values are attributed to delivering enhanced device performances. The fabricated OLEDs manifested a high EQE of 12% for the **DHPZ-2BI** material, which is better compared to simple conventional fluorescent molecules. Even though the color point of view, the advantageous orange region achieved, which is a better sign compared to carbazole-based A–D–A type TADF motifs, the EQE is limited in this design. However, the phenazine based donor can advance the A–D–A type TADF materials with suitable acceptor motifs.

Karthik *et al.* introduced two novel orange-red TADF materials, **PzTDBA** and **PzDBA**, to extend this A–D–A type design. The **PzTDBA** contains two *tert*-butyl substituted **DOBNA** acceptors (**TDBA**), whereas **PzDBA** has two **DOBNA** moieties with the same dihydrophenazine as the donor.<sup>82</sup> Both materials showed extremely small  $\Delta E_{ST}$  of less than 0.06 eV, indicating the superiority of TADF characteristics. Furthermore, the exciton delayed lifetime manifested less than 2.63  $\mu$ s in 5 wt% doped films. Due to the high molecular rigid acceptor units, both materials showed high PLQY of near unity (100%). With the support of a short delayed lifetime and small  $\Delta E_{ST}$  values, both materials manifested high RISC rate constant values in the order of  $10^6$  s<sup>-1</sup>. Initially, the TADF-OLEDs were fabricated with the help of a **CBP** host in a variation of different doping concentrations. Among all devices, the 5 wt% based TADF emitters achieved high EQE of 30.3% (**PzTDBA**) and 21.8% (**PzDBA**), respectively. The EQE is still maintained at 28.4% for **PzTDBA** and 20.1% for **PzDBA** even at 3000 cd m<sup>-2</sup>. Consequently, the **PzTDBA** showed orange-red emission with  $EL_{max}$  of 576 nm, whereas **PzDBA** manifested red emission at 595 nm with alleviated efficient roll-off characteristics. This A–D–A type design indicates that the highly rigid moieties can enhance the stability of the TADF materials. Moreover, it was confirmed that such ultra-roll-off features are obtained due to the suppression of exciton annihilation quenching with the support of a high RISC rate and short exciton delayed lifetime. Furthermore, both materials showed high horizontal dipole orientations due to the extended A–D–A molecular designs. Ultimately, the TADF-OLEDs manifested a long operational life of 159/193 hours for **PzTDBA/PzDBA** at 1000 cd m<sup>-2</sup>. Even though EQE is higher for **PzTDBA**, the lifetime is shorter than **PzDBA** due to the weak bond dissociation energy (BDE) of the **TDBA** acceptor in the **PzTDBA** molecule. This design indicates the high superiority of the A–D–A type TADF molecules for developing highly efficient OLEDs in red-shifted regions, thereby advancing the growing optoelectronic fields.

Recently, Can Zhong Lu *et al.* developed three A–D–A based TADF materials: **QxPz**, **DMQxPz**, and **DPQxPz** based on the quinoxaline-derived acceptors with the same 5,10-disubstituted phenazine as the donor.<sup>88</sup> Usually, the longer wavelength (over the orange color) region TADF materials encounter significant nonradiative decay issues based on the energy-gap law, leading

to relatively large  $\Delta E_{ST}$  and compromising efficient up-conversion.<sup>89</sup> But in this design, the developed materials showed tiny  $\Delta E_{ST}$  due to the substantial CT character due to their symmetrical A–D–A configuration and ladder rod-like chemical structures, resulting in high PLQY values of up to 85% and the enhanced RISC process. Among the developed materials, the **DMQxPz** manifested an immense RISC constant value of  $1.23 \times 10^6$  s<sup>-1</sup> and a PLQY of 85% in a 3 wt%-doped **CBP** film. Then the TADF emitters are embedded in doped OLEDs, which showed high EQE values near almost 20% with moderate EQE roll-off values in orange to red electroluminescence. Such low roll-off properties are due to the short exciton lifetime and fast RISC rate values. Furthermore, the OLEDs showed an impressive luminance value of 31 240 cd m<sup>-2</sup>, indicating molecular rigidity with steric hindrance based A–D–A type designs. These findings demonstrate the potential of 5,10-disubstituted phenazine electron donors in constructing highly efficient red TADF emitters based on A–D–A type designs. This study also provides an effective strategy for rationalizing excited states through structural engineering, opening up exciting possible molecular designs for future advancements in OLED displays.

Very recently, Tang *et al.* unveiled the same A–D–A design similar to **PzTDBA** materials reported by Karthik *et al.*<sup>82</sup> But here, authors utilized Pure MR-TADF rigid B, N-type core in place of acceptor and developed two orange-red TADF emitters, namely, **2BNCz-PZ** and **2BNtCz-PZ**, by bearing the same dihydrophenazine donor.<sup>90</sup> These materials showed hybrid LR/SR CT characters, which allow them to manifest the small  $\Delta E_{ST}$ , immense oscillator strength ( $f$ ), high PLQY, short exciton delayed lifetime, and high RISC rate over  $10^6$  s<sup>-1</sup>. The rod-like A–D–A configuration and disk-like segments will efficiently enhance the horizontal dipole orientation ( $\theta_{||}$ ) values for improved light extraction. A tiny  $\Delta E_{ST}$  of 0.04 and 0.02 eV, a short microsecond-scale  $\tau_d$  of 1.5 and 1.4  $\mu$ s, a high  $\Phi_{PL}$  of 96% and 93%, and a high  $\theta_{||}$  of 86% and 91% were accomplished, respectively. These values indicate that both materials can manifest high TADF properties. Furthermore, the obtained horizontal emitting dipole orientation factor is over 90%, which is very high among the developed A–D–A type TADF materials. Such high values are due to the enhanced transition dipole moment and rod-like A–D–A-based designs. Then the fabricated OLEDs based on **2BNtCz-PZ** revealed a high EQE of 31% with a slight EQE roll-off at 22.2% in 1000 cd m<sup>-2</sup>. Furthermore, the devices showed an emission maximum of over 600 nm with bright red electroluminescence properties. Then due to the use of orange-red dopants with an intense charge-transfer absorption band, the white OLEDs based on a single emitting layer achieved high maximum EQE of 30.6%, indicating the superiority of molecular designs. This work reveals the potential of utilizing the rod-like A–D–A design configuration to construct high-performance orange-red TADF emitters with ultra-roll-off EQE characteristics. The detailed structure–property with the effect of donor and acceptors in boron based A–D–A type TADF emitters are depicted in Fig. 5.

On the other hand, the same group developed a rigid emitter (**2PXZ-2TRZ**) with a three-dimensional dislocated sandwich

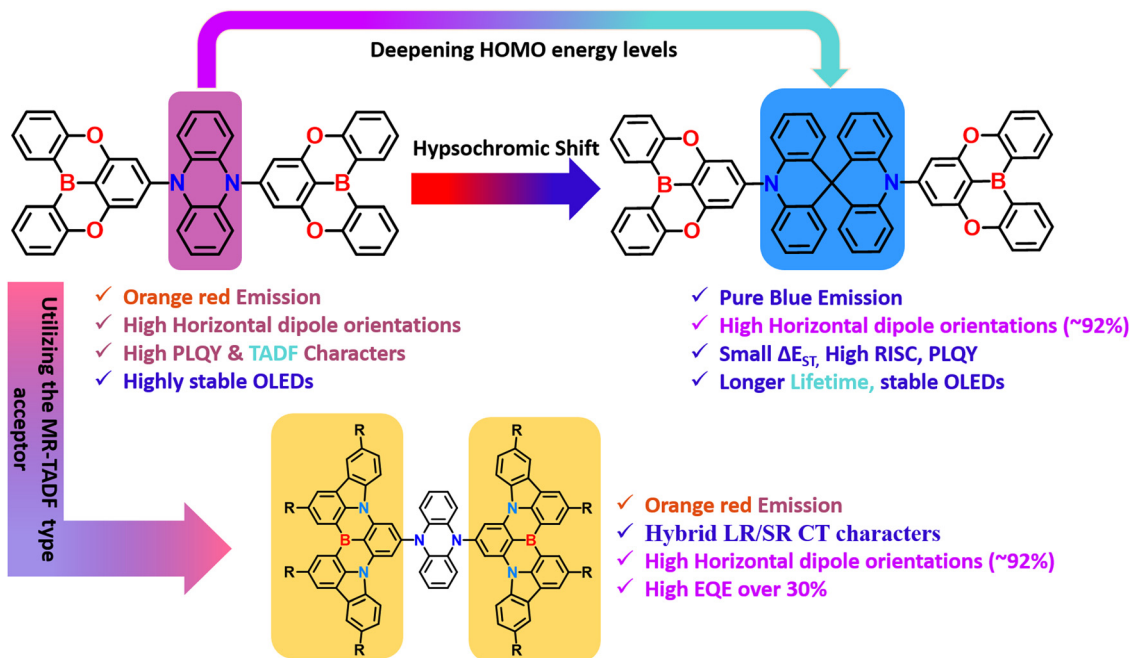


Fig. 5 Comparison of the effect of donor and acceptors in boron based A-D-A type TADF emitters.

A-D-A configuration by linking bi-phenazine (2PXZ) donor and 2,4,6-triphenyl-1,3,5-triazine (TRZ) acceptor through the twin-locking of two spiro-fluorene bridges.<sup>91</sup> This twin-locking strategy enables them to show through space CT characteristics and effectively inhibit the intramolecular twisting and stretching vibrations, facilitating the suppressed non-radiative decay and fast RISC process. The 2PXZ-2TRZ was successfully synthesized by a sequential one-pot method of nucleophilic addition and acid-catalyzed cyclization. Consequently, the emitter shows green emission with a small  $\Delta E_{ST}$  value of 0.01 eV, a short delayed exciton lifetime of 5.3  $\mu\text{s}$ , and a high RISC rate of  $6.0 \times 10^5 \text{ s}^{-1}$ . These properties indicate that the 2PXZ-2TRZ can show efficient TADF characteristics. Furthermore, this molecule showed AIE behavior also. Fabricated OLEDs revealed  $\text{EQE}_{\text{max}}$  of 27.1% with alleviated roll-off characteristics at high luminance values. There is no information related to the horizontal

dipole orientation values. This work indicates the crucial role of utilizing the bi-phenazine-type donor, which can show the AIE and TADF properties together.

### 2.3. Spiro-biacridine based donors in A-D-A based TADF materials

Like phenazine-based donors, several spiro-biacridine-based donors also utilized A-D-A-based TADF designs. Initially, Kim *et al.* reported blue TADF emitter **DBA-SAB** based on an A-D-A type design (Fig. 6).<sup>17</sup> The **DBA-SAB** is similar to **PzDBA**,<sup>82</sup> but the donor is changed from Phenazine to spiro-biacridine, which weakens the conjugation effect and deep HOMO energy level, leading to blue-shifted emission compared to **PzDBA**. The **DBA-SAB** contains two **DOBNA** moieties as acceptors and one spiro-biacridine as a donor in the A-D-A configuration. Since the rigid donor and acceptor motifs exist, the **DBA-SAB** manifested

#### SpiroAcridine donor based A-D-A TADF cores

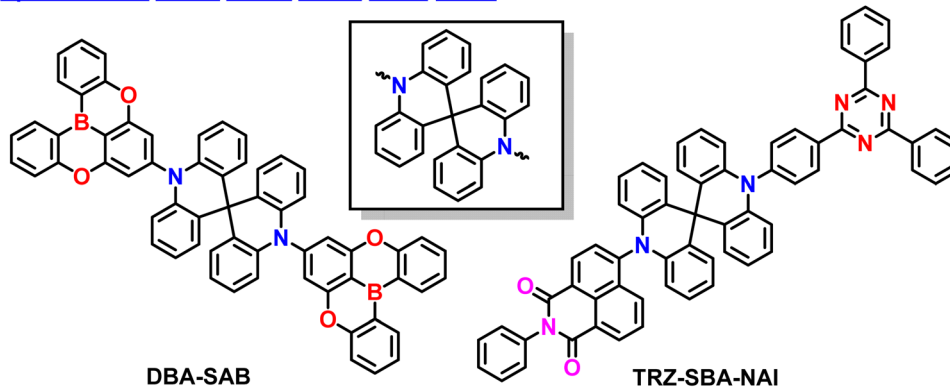


Fig. 6 Chemical structures discussed in the spiro-biacridine donor of A-D-A type TADF materials.



narrowband emission spectra, which is keen for future displays reaching towards the BT2020 standards.<sup>73,92</sup> Then **DBA-SAB** also reveals a small  $\Delta E_{ST}$  value of 0.07 eV, a short delayed exciton lifetime of 0.96  $\mu\text{s}$ , and a high RISC rate of  $1.9 \times 10^6 \text{ s}^{-1}$ . These properties indicate that the **DBA-SAB** can show efficient TADF characteristics. Moreover, the PLQY also reached nearly 90%, which shows the A–D–A designs' superiority. Similar to the literature mentioned earlier, this **DBA-SAB** also showed a high horizontal dipole orientation ratio of 89% due to the rod-like long molecular structure along the transition dipole moment direction. These combined effects led to the development of high-performance blue OLEDs. The fabricated OLEDs based on **DBA-SAB** manifested a high EQE of 25.7% with CIE coordinates of (0.144, 0.212). Furthermore, the EQE is maintained at 23.6% even at  $1000 \text{ cd m}^{-2}$ , indicating the greatness of the molecular A–D–A type designs. These EQE values emphasize that pure blue high-performance OLEDs can be achieved by utilizing the weakened donating ability.

Even though several studies have been reported to date, all the materials contain similar acceptor moieties, making them symmetrical TADF molecular skeletons. Recently, Chuluo Yang *et al.* unveiled an unsymmetrical A–D–A' design incorporating 2-phenyl-1*H*-benzo[*de*] isoquinoline-1,3(2*H*)-dione and 2,4,6-triphenyl-1,3,5-triazine as acceptor moieties into a spirobisacridine donor.<sup>93</sup> This is the first report based on an unsymmetrical A–D–A' type TADF design. Due to the dual accepting abilities, the **TRZ-SBA-NAI** manifested unique dual emission properties with an orange-red emission and a sky-blue shoulder emission peak in the solution state. Such behavior is likely due to the double charge-transfer excited states from both different acceptors. Furthermore, when doped into a host matrix, the **TRZ-SBA-NAI** showed a high PLQY of 87% with an orange-red emission. As an ongoing discussion related to linear rod-like structures, this molecule also showed a high horizontal dipole ratio of 88%, which is relatively high compared to the conventional D–A based TADF emitters. The fabricated OLEDs revealed excellent electroluminescence performances with a maximum EQE of 31.7%, an EL peak at 593 nm, and intense orange-red emission. The corresponding CIE coordinates are (0.55, 0.45), near the red region of BT2020 standards. Due to the

enhanced orientation factor, the optical outcoupling efficiency reached nearly 40%, indicating the superiority of the unsymmetrical molecular A–D–A' design. This finding expands the diversity in TADF molecular design and unlocks the tremendous potential of A–D–A' type TADF emitters in achieving exceptional device performance. The discovery of **TRZ-SBA-NAI** highlights the enormous potential of A–D–A' type TADF emitters for advancing high-efficiency OLEDs. The researchers continue their efforts to prepare versatile TADF emitters, paving the way for further advancements in this exciting field of research.

#### 2.4. Imidazole based core in A–D–A based materials

In 2016, Yang *et al.* reported V-shaped molecules based on the A–D–A designs. The developed molecule, **TPA-2PPI** have one triphenylamine donor and two 1-phenyl-2-(4-(4,4,5,5-tetramethyl-1,3,2-dioxaborolan-2-yl)phenyl)-1*H*-phenanthro[9,10-*d*]imidazole acted as acceptors (Fig. 7).<sup>94</sup> This molecule manifests hybrid local and charge-transfer (HLCT) excited state property from low polar to high polar solvents. However, the **TPA-2PPI** showed higher thermal stability than simple D–A-based material (**TPA-PPI**). Even though it showed high stability, it does not contain any TADF properties, suggesting its use as a fluorescent A–D–A-based material. The non-doped OLED device based on **TPA-2PPI** emitter exhibits a deep blue emission spectrum, peaking at 452 nm with a narrow FWHM of only 50 nm and CIE coordinates of (0.151, 0.108). The device performance is reasonably excellent for fluorescent devices, with a maximum EQE of 4.91% and maximum current efficiency (CE) of  $4.76 \text{ cd A}^{-1}$ . Importantly, the device also shows a very slow roll-off of EQE (or CE) with values maintained at 4.89% (or  $4.74 \text{ cd A}^{-1}$ ) and 4.56% (or  $4.42 \text{ cd A}^{-1}$ ) within a practical luminance range of 100 to  $1000 \text{ cd m}^{-2}$ . This slow roll-off of efficiency is beneficial for enhancing the operative stability of OLED devices. This study not only proposes a novel molecular design for high-efficiency deep-blue OLED materials using the HLCT mechanism but also provides a feasible method to enhance OLED device stability by increasing the thermal stability of the materials. These molecular designs can be further modified with donor and acceptor components to boost the OLED performances further.

#### Imidazole based A–D–A TADF cores

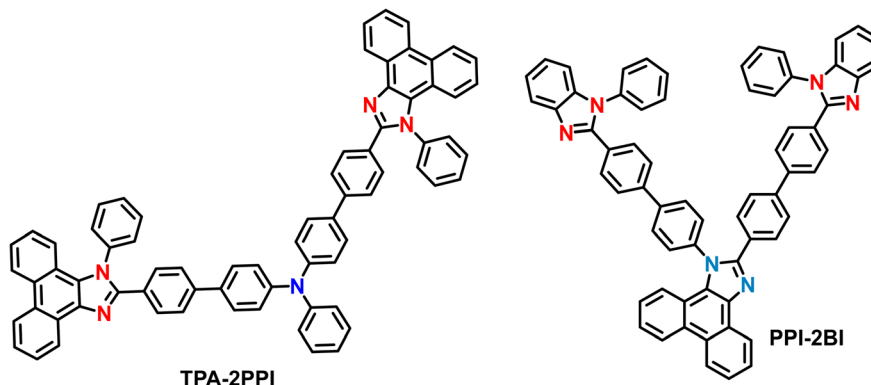


Fig. 7 Chemical structures discussed in the imidazole based core of A–D–A type TADF materials.

Tao *et al.* unveiled a triangular A–D–A molecular design and developed an asymmetrically twisted deep-blue emitting molecule **PPI-2BI**.<sup>95</sup> The **PPI-2BI** contains a phenanthroimidazole (PI) donor unit with two electrophilic benzimidazole (BI) units attached at the C2 and N1 positions. The **PPI-2BI** manifested improved electron injecting and transporting abilities due to the enhanced D–A electronic coupling in the core, which even shows high PL and EL properties. However, similar to **TPA-2PPI**, this material also does not offer any TADF properties. By utilizing the **PPI-2BI** as an emitting layer, the multilayer OLEDs revealed a high EQE of 4.63%, a current efficiency (CE) of 4.98 cd A<sup>-1</sup>, a power efficiency (PE) of 4.82 lm W<sup>-1</sup>, and CIE coordinates of (0.158, 0.124) in the pure blue region (EL<sub>max</sub>: 452 nm). Furthermore, when the doped device is fabricated, the **PPI-2BI** manifested efficient near-ultraviolet EL with color coordinates of (0.154, 0.047) and an EQE of 4.12%, which is comparable to the best-reported near-UV emitting devices. The corresponding CIE coordinates are almost reached the NTSC

and BT2020 requirements. These results showcase the successful design of a novel molecular structure for bifunctional deep-blue emitters and offer a new strategy for building such emitters with enhanced efficiencies. The advancements in **PPI-2BI** as a high-performance deep-blue fluorescent molecule hold promising applications in optoelectronic devices and display technologies.

## 2.5. Other types of A–D–A based materials

Shi *et al.* have successfully developed and synthesized four novel carbazole/oxadiazole hybrid molecules using a straightforward catalyst-free C–N coupling reaction. The rational molecular design approach for all ortho-linked carbazole/oxadiazole (Cz/OXD) hybrids, where they adjusted the numbers of donor/acceptor units and electron-donating abilities to achieve tunable D–A interactions (Fig. 8).<sup>96</sup> By utilizing the multidonors in the A–D–A design (**4CzDOXD** and **4tCzDOXD**), the TADF nature has been improved due to their efficient FMO separation.

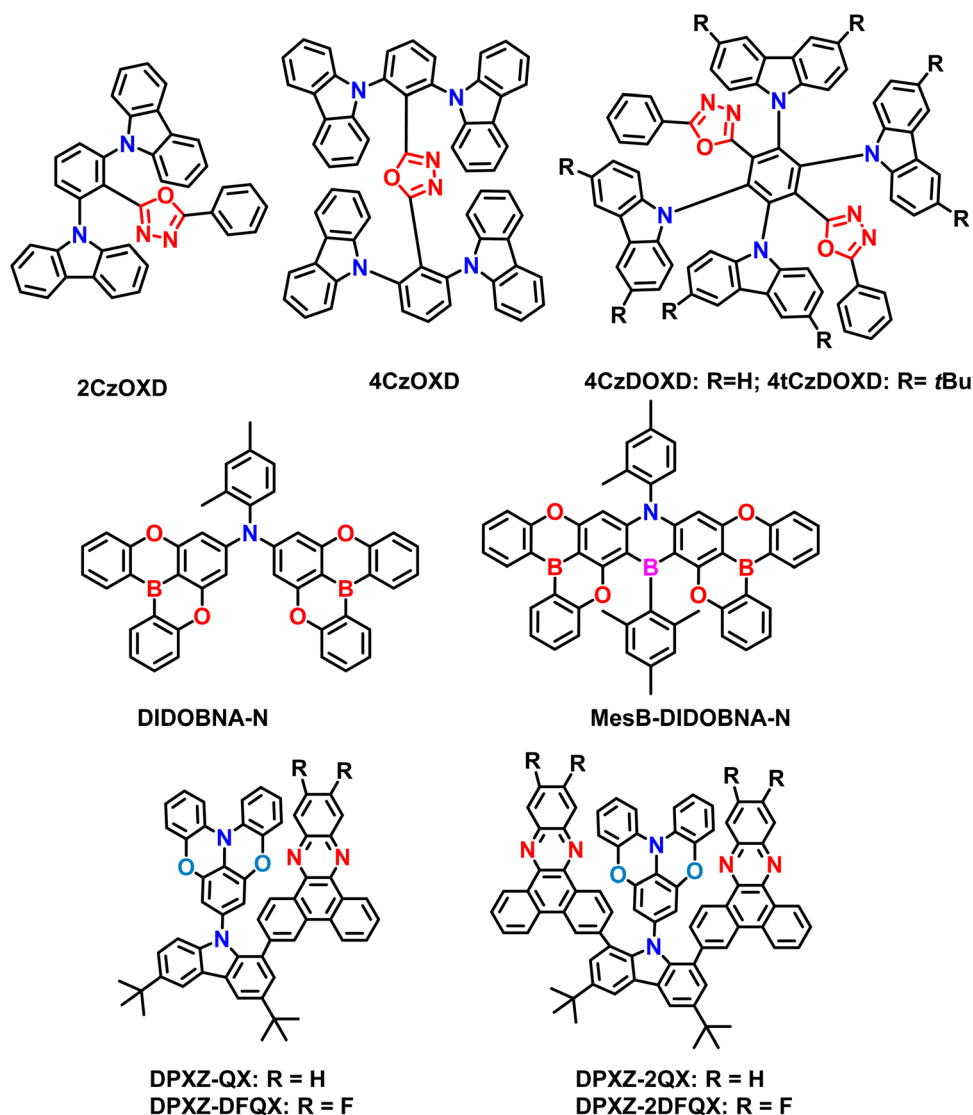


Fig. 8 Chemical structures discussed in other types of A–D–A type materials.

Subsequently, they achieved a small  $\Delta E_{ST}$  close to 0 for A–D–A based compounds. The D–A and D–A–D type compounds, namely **2CzOXD** and **4CzOXD**, were also synthesized for comparison. However these materials did not show any TADF behavior and resulted in PLQY of less than 10%. However, the A–D–A based materials showed strong TADF properties with high PLQYs ranging from 71% (**4CzDOXD**) to 92% (**4tCzDOXD**). Such improved PLQY values are due to the insertion of *tert*butyl groups in the carbazole moiety. Due to the small  $\Delta E_{ST}$  values, the RISC rate is also efficient compared to D–A/D–A–D type materials (**2CzOXD** and **4CzOXD**). Furthermore, the A–D–A type compounds **4CzDOXD** and **4tCzDOXD** demonstrated a high EQE ranging from 19.4% to 22.6% in OLEDs. The successful outcome of these compounds highlights the potential for designing highly efficient TADF materials for practical applications. To support their findings, the researchers also conducted theoretical calculations, which provided valuable guidance for designing future efficient A–D–A based TADF materials.

Recently, Colmon *et al.* utilized two **DOBNA** moieties attached to the methyl-annulated aniline, making it an A–D–A type TADF material **DIDOBNA-N**.<sup>97</sup> Then the **DIDOBNA-N** was further borylated to make it an efficient MR-TADF material **MesB-DIDOBNA-N**. Due to the increasing accepting ability, **MesB-DIDOBNA-N** showed near-UV emission compared to the **DIDOBNA-N**, which revealed deep blue emission. The 1.5 wt% of **DIDOBNA-N** manifested a high PLQY of 81% and  $\tau_d = 23$  ms in the **TSPO1** host matrix. On the other hand, the **MesB-DIDOBNA-N** showed narrowband near UV-emission ( $\lambda_{PL} = 402$  nm, FWHM = 19 nm) with relatively low PLQY of 75% and  $\tau_d = 133$   $\mu$ s, indicating the near UV-MR-TADF material. Then the fabricated OLEDs manifested EQE<sub>max</sub> of 15.3% (**DIDOBNA-N**) and 16.2% (**MesB-DIDOBNA-N**) in pure blue, deep blue electroluminescence. There is no information on the horizontal dipole orientation for both materials. Notably, the CIE *y* coordinates have almost reached the BT2020 blue standards. This indicates the superiority of structural transformation from **DIDOBNA-N** to **MesB-DIDOBNA-N**, involving the installation of a bridging mesitylated borane unit, significantly blue-shifts and narrows the emission. **MesB-DIDOBNA-N** represents a rare example of a non-triangular type  $\pi$ -extended near-UV MR-TADF emitter. The findings from this study hold great promise not only for near-UV light sources but also for materials design in high-performance near-UV emitters, which can have applications in sensing, photochemistry, high-density information storage, medicine, and sterilization. Developing such efficient MR-TADF emitters opens up new possibilities for various advancements.

Usually, minimizing the band gap, which leads to more prolonged wavelength emission, is challenging to design with through-space charge transfer (TSCT) properties. Recently, Kai Li *et al.* unveiled the A–D–A design to build the TSCT excited states with efficient TADF properties.<sup>98</sup> The developed scaffolds, namely, **DPXZ-QX**, **DPXZ-DFQX**, **DPXZ-2QX**, and **DPXZ-2DFQX**, contain planar dibenzo[*a,c*]phenazine (QX) and its fluorinated derivative (DFQX) as the acceptors. Among them, the **DPXZ-2QX** and **DPXZ-2DFQX** are combinations of A–D–A

type designs, whereas the rest are D–A combinations. Notably, both materials (**DPXZ-2QX** and **DPXZ-2DFQX**) manifested the red emission around 600 nm,  $\Delta E_{ST}$  below 0.02, and high PLQY over 87%. These characteristics indicate that they can show high TADF properties. Such high TADF properties are due to the sandwich-shaped A–D–A combinations in a cofacial manner. Furthermore, the delayed fluorescence lifetimes are as short as 4.9  $\mu$ s in doped thin films, which confirms the TADF characters again. Due to the strong intramolecular  $\pi$ -stacking interactions with the presence of dual acceptors, it can contribute to the TSCT-TADF emissions. Furthermore, the fabricated OLEDs based on these new A–D–A emitters showcased electroluminescence with maximum EQEs of up to 23.2% for the red TSCT-TADF emitters. Notably, achieving an EQE of 18.9% at a brightness of 1000 cd m<sup>-2</sup> represents one of the highest values for red TADF OLEDs. Such values are due to the extremely small  $\Delta E_{ST}$ , high PLQY, and short exciton delayed lifetime. Overall, mainly the molecular design of these A–D–A-based emitters relies on confining rigid and (quasi)planar donor-acceptor(s) in a face-to-face orientation, promoting strong intramolecular  $\pi$ -stacking interactions within the donor-acceptor pair. This arrangement ensures a simultaneous enhancement of radiative charge transfer transition and suppression of non-radiative decay. Additionally, regulating the RISC rate through multiple acceptors in an A–D–A emitter with a sandwich configuration further contributes to high-performance red OLEDs with a small efficiency roll-off. This study underscores the importance of controlling the conformation and orientation of donor-acceptor pairs for designing high-efficiency TSCT-TADF emitters. Incorporating intramolecular cofacial  $\pi$ -stacking interactions offers a modular approach for developing full-color, high-performance TADF emitters.

### 3. Summary and outlook

With the great advent of  $\sim 100\%$  exciton utilization efficiency for light emission without noble metals, significant efforts have been devoted to developing TADF emitters for OLEDs. Growingly, the EQE of the TADF emitters reached the level of phosphorescent emitters and was considered a potential alternative to the existing light-emitting technologies. Among the reported many TADF emitters, A–D–A type TADF materials are superior due to the rod-like structures and favorable dipole orientations for efficient light harvesting. Usually, aggregation caused quenching (ACQ) is a common problem in planar moieties embedded in A–D–A type TADF materials, which leads to intermolecular interactions and results in non-radiative decay pathways. This phenomenon can significantly reduce the TADF efficiency and compromise the performance of OLED devices. However, TSCT materials with slightly twisted configurations can mitigate these ACQ issues and manifest efficient OLED devices. However, there are only limited reports on A–D–A-based designs. On the other hand, stability under electrical stress is one of the critical parameters which needs to be addressed. Usually, high current densities and electrical stress lead to device degradation and reduce the

operational lifetime of the OLEDs. Currently, there are vast developments with the help of host matrices in A–D–A based TADF materials using appreciative charge injection and transportation, which reduce the triplet-polaron quenching and enhance device reliability. In recent days, the MR-TADF devices are mostly showing EQE roll-off characteristics. However, without compromising the color purity, designing A–D–A-based MR-TADF material based on elongation strategies and weakening donating strength can be an excellent MR-based candidate for the narrow-band OLEDs. Currently, among the developed materials, the 2BOICz manifested a high EQE of 40.4% in the green region due to the enhanced dipole orientation with dual CT characteristics. Then TRZ-SBA-NAI, with an unsymmetrical pattern, showed red emission with a high EQE of 31.7%, making another pathway towards longer wavelength TADF materials. However, there are limited materials in blue emission, so by considering the future aspects, new molecular designs must be needed for efficient TADF-OLED performances. However, by adopting the straightforward molecular strategy based on MR cores with very weak donating abilities would result in elongated conjugation and enhanced MR effect (showing narrowband), which can be a new pathway to improve the horizontal dipole orientation in MR-TADF skeletons mainly used in blue OLEDs.

On the other hand, the integration of machine learning and computational technologies for new material design has shown great potential in accelerating the discovery of novel TADF emitters in recent days. With the limited examples of A–D–A designs, Looking ahead, emerging trends in A–D–A-based TADF materials, including advancements in blue-emitting materials, would be a plus, as blue OLEDs are crucial for full-color displays and lighting applications. Additionally, efforts to achieve color-tunable emitters based on ADA structures offer exciting prospects for adaptable and dynamic OLED displays. Integrating ADA-based TADF materials with other cutting-edge technologies, such as flexible substrates and wearable electronics, opens up new avenues for diverse OLED applications in smart devices and the Internet of Things (IoT). Furthermore, ongoing research on large-area and solution-processed OLED fabrication techniques may lead to more cost-effective and scalable manufacturing processes for ADA-based TADF devices with novel new molecules, further driving their commercial viability. As the OLED industry advances, ADA-based TADF materials are expected to play a vital role due to their high horizontal dipole orientation factors in shaping the future of displays, lighting, and various emerging applications, making them a prominent contender in the next generation of OLED technology.

## Author contributions

CPKP and KRN contributed to writing and revising of this manuscript. Both KRN and JH equally supervised this work. All authors listed have made a substantial, direct and intellectual contribution to the work, and approved it for publication.

## Conflicts of interest

All the authors declare no competing financial interest.

## Acknowledgements

This research was supported by the Basic Science Research Capacity Enhancement Project through the Korea Basic Science Institute (National Research Facilities and Equipment Center) grant funded by the Ministry of Education (2019R1A6C1010016) and the Korea Institute for Advancement of Technology (KIAT) grant funded by the Korea Government (MOTIE) (P0012451, the Competency Development Program for Industry Specialist).

## References

- 1 C. W. Tang and S. A. VanSlyke, Organic electroluminescent diodes, *Appl. Phys. Lett.*, 1987, **51**, 913–915.
- 2 J. Zou, H. Wu, C.-S. Lam, C. Wang, J. Zhu, C. Zhong, S. Hu, C.-L. Ho, G.-J. Zhou, H. Wu, W. C. H. Choy, J. Peng, Y. Cao and W.-Y. Wong, Simultaneous Optimization of Charge-Carrier Balance and Luminous Efficacy in Highly Efficient White Polymer Light-Emitting Devices, *Adv. Mater.*, 2011, **23**, 2976–2980.
- 3 Y. Sun, N. C. Giebink, H. Kanno, B. Ma, M. E. Thompson and S. R. Forrest, Management of singlet and triplet excitons for efficient white organic light-emitting devices, *Nature*, 2006, **440**, 908–912.
- 4 S. Reineke, F. Lindner, G. Schwartz, N. Seidler, K. Walzer, B. Lüssem and K. Leo, White organic light-emitting diodes with fluorescent tube efficiency, *Nature*, 2009, **459**, 234–238.
- 5 H. I. Yang, K. R. Naveen, S. M. Cho, J. Y. Kim, Y. H. Jung and J. H. Kwon, Systematic investigation on polymer layer selection for flexible thin film encapsulation, *Org. Electron.*, 2023, **115**, 106761.
- 6 H. Sasabe and J. Kido, Recent Progress in Phosphorescent Organic Light-Emitting Devices, *Eur. J. Org. Chem.*, 2013, 7653–7663.
- 7 C. Adachi, M. A. Baldo, M. E. Thompson and S. R. Forrest, Nearly 100% internal phosphorescence efficiency in an organic light-emitting device, *J. Appl. Phys.*, 2001, **90**, 5048–5051.
- 8 K.-H. Kim, S. Lee, C.-K. Moon, S.-Y. Kim, Y.-S. Park, J.-H. Lee, J. Woo Lee, J. Huh, Y. You and J.-J. Kim, Phosphorescent dye-based supramolecules for high-efficiency organic light-emitting diodes, *Nat. Commun.*, 2014, **5**, 4769.
- 9 H. Uoyama, K. Goushi, K. Shizu, H. Nomura and C. Adachi, Highly efficient organic light-emitting diodes from delayed fluorescence, *Nature*, 2012, **492**, 234–238.
- 10 Y. Tao, K. Yuan, T. Chen, P. Xu, H. Li, R. Chen, C. Zheng, L. Zhang and W. Huang, Thermally Activated Delayed Fluorescence Materials Towards the Breakthrough of Organoelectronics, *Adv. Mater.*, 2014, **26**, 7931–7958.
- 11 V. Daniel, Review of organic light-emitting diodes with thermally activated delayed fluorescence emitters for energy-efficient sustainable light sources and displays, *J. Photonics Energy*, 2016, **6**, 020901.



- 12 Y. Gawale, R. Ansari, K. R. Naveen and J. H. Kwon, Forthcoming hyperfluorescence display technology: relevant factors to achieve high-performance stable organic light emitting diodes, *Front. Chem.*, 2023, **11**, 1211345.
- 13 B. Minaev, G. Baryshnikov and H. Agren, Principles of phosphorescent organic light emitting devices, *Phys. Chem. Chem. Phys.*, 2014, **16**, 1719–1758.
- 14 Y. Xiao, H. Wang, Z. Xie, M. Shen, R. Huang, Y. Miao, G. Liu, T. Yu and W. Huang, NIR TADF emitters and OLEDs: challenges, progress, and perspectives, *Chem. Sci.*, 2022, **13**, 8906–8923.
- 15 X. Yin, Y. He, X. Wang, Z. Wu, E. Pang, J. Xu and J.-A. Wang, Recent Advances in Thermally Activated Delayed Fluorescent Polymer—Molecular Designing Strategies, *Front. Chem.*, 2020, **8**, 725.
- 16 M. Y. Wong and E. Zysman-Colman, Purely Organic Thermally Activated Delayed Fluorescence Materials for Organic Light-Emitting Diodes, *Adv. Mater.*, 2017, **29**, 1605444.
- 17 H. Lim, H. J. Cheon, S.-J. Woo, S.-K. Kwon, Y.-H. Kim and J.-J. Kim, Highly Efficient Deep-Blue OLEDs using a TADF Emitter with a Narrow Emission Spectrum and High Horizontal Emitting Dipole Ratio, *Adv. Mater.*, 2020, **32**, 2004083.
- 18 Y. H. Lee, S. Park, J. Oh, S.-J. Woo, A. Kumar, J.-J. Kim, J. Jung, S. Yoo and M. H. Lee, High-Efficiency Sky Blue to Ultradeep Blue Thermally Activated Delayed Fluorescent Diodes Based on Ortho-Carbazole-Appended Triarylboron Emitters: Above 32% External Quantum Efficiency in Blue Devices, *Adv. Opt. Mater.*, 2018, **6**, 1800385.
- 19 Y.-K. Chen, J. Jayakumar, C.-M. Hsieh, T.-L. Wu, C.-C. Liao, J. Pandidurai, C.-L. Ko, W.-Y. Hung and C.-H. Cheng, Triarylamine-Pyridine-Carbonitriles for Organic Light-Emitting Devices with EQE Nearly 40%, *Adv. Mater.*, 2021, **33**, 2008032.
- 20 Y. Wada, S. Kubo and H. Kaji, Adamantyl Substitution Strategy for Realizing Solution-Processable Thermally Stable Deep-Blue Thermally Activated Delayed Fluorescence Materials, *Adv. Mater.*, 2018, **30**, 1705641.
- 21 H. Shin, Y. H. Ha, H.-G. Kim, R. Kim, S.-K. Kwon, Y.-H. Kim and J.-J. Kim, Controlling Horizontal Dipole Orientation and Emission Spectrum of Ir Complexes by Chemical Design of Ancillary Ligands for Efficient Deep-Blue Organic Light-Emitting Diodes, *Adv. Mater.*, 2019, **31**, 1808102.
- 22 D. Zhang, X. Song, A. J. Gillett, B. H. Drummond, S. T. E. Jones, G. Li, H. He, M. Cai, D. Credgington and L. Duan, Efficient and Stable Deep-Blue Fluorescent Organic Light-Emitting Diodes Employing a Sensitizer with Fast Triplet Upconversion, *Adv. Mater.*, 2020, **32**, 1908355.
- 23 S. Nam, J. W. Kim, H. J. Bae, Y. M. Maruyama, D. Jeong, J. Kim, J. S. Kim, W.-J. Son, H. Jeong, J. Lee, S.-G. Ihn and H. Choi, Improved Efficiency and Lifetime of Deep-Blue Hyperfluorescent Organic Light-Emitting Diode using Pt(II) Complex as Phosphorescent Sensitizer, *Adv. Sci.*, 2021, **8**, 2100586.
- 24 G. Hong, X. Gan, C. Leonhardt, Z. Zhang, J. Seibert, J. M. Busch and S. Bräse, A Brief History of OLEDs—Emitter Development and Industry Milestones, *Adv. Mater.*, 2021, **33**, 2005630.
- 25 M. Vasilopoulou, A. Fakharuddin, F. P. García de Arquer, D. G. Georgiadou, H. Kim, A. R. B. Mohd Yusoff, F. Gao, M. K. Nazeeruddin, H. J. Bolink and E. H. Sargent, Advances in solution-processed near-infrared light-emitting diodes, *Nat. Photonics*, 2021, **15**, 656–669.
- 26 Y.-Z. Shi, H. Wu, K. Wang, J. Yu, X.-M. Ou and X.-H. Zhang, Recent progress in thermally activated delayed fluorescence emitters for nondoped organic light-emitting diodes, *Chem. Sci.*, 2022, **13**, 3625–3651.
- 27 R. K. Konidena and K. R. Naveen, Boron-Based Narrowband Multiresonance Delayed Fluorescent Emitters for Organic Light-Emitting Diodes, *Adv. Photonics Res.*, 2022, **3**, 2200201.
- 28 R. Braveenth, H. Lee, J. D. Park, K. J. Yang, S. J. Hwang, K. R. Naveen, R. Lampande and J. H. Kwon, Achieving Narrow FWHM and High EQE Over 38% in Blue OLEDs Using Rigid Heteroatom-Based Deep Blue TADF Sensitized Host, *Adv. Funct. Mater.*, 2021, **31**, 2105805.
- 29 H. Nakanotani, Y. Tsuchiya and C. Adachi, Thermally-activated Delayed Fluorescence for Light-emitting Devices, *Chem. Lett.*, 2021, **50**, 938–948.
- 30 K. R. Naveen, H. I. Yang and J. H. Kwon, Double boron-embedded multiresonant thermally activated delayed fluorescent materials for organic light-emitting diodes, *Commun. Chem.*, 2022, **5**, 149.
- 31 J.-H. Lee, C.-H. Chen, P.-H. Lee, H.-Y. Lin, M.-K. Leung, T.-L. Chiu and C.-F. Lin, Blue organic light-emitting diodes: current status, challenges, and future outlook, *J. Mater. Chem. C*, 2019, **7**, 5874–5888.
- 32 Q. Zhang, J. Li, K. Shizu, S. Huang, S. Hirata, H. Miyazaki and C. Adachi, Design of Efficient Thermally Activated Delayed Fluorescence Materials for Pure Blue Organic Light Emitting Diodes, *J. Am. Chem. Soc.*, 2012, **134**, 14706–14709.
- 33 H. Nakanotani, T. Higuchi, T. Furukawa, K. Masui, K. Morimoto, M. Numata, H. Tanaka, Y. Sagara, T. Yasuda and C. Adachi, High-efficiency organic light-emitting diodes with fluorescent emitters, *Nat. Commun.*, 2014, **5**, 4016.
- 34 H. Kaji, H. Suzuki, T. Fukushima, K. Shizu, K. Suzuki, S. Kubo, T. Komino, H. Oiwa, F. Suzuki, A. Wakamiya, Y. Murata and C. Adachi, Purely organic electroluminescent material realizing 100% conversion from electricity to light, *Nat. Commun.*, 2015, **6**, 8476.
- 35 Z. Yang, Z. Mao, Z. Xie, Y. Zhang, S. Liu, J. Zhao, J. Xu, Z. Chi and M. P. Aldred, Recent advances in organic thermally activated delayed fluorescence materials, *Chem. Soc. Rev.*, 2017, **46**, 915–1016.
- 36 V. Jankus, C.-J. Chiang, F. Dias and A. P. Monkman, Deep Blue Exciplex Organic Light-Emitting Diodes with Enhanced Efficiency; P-type or E-type Triplet Conversion to Singlet Excitons?, *Adv. Mater.*, 2013, **25**, 1455–1459.
- 37 T. J. Penfold, E. Gindensperger, C. Daniel and C. M. Marian, Spin-Vibronic Mechanism for Intersystem Crossing, *Chem. Rev.*, 2018, **118**, 6975–7025.
- 38 S. Y. Lee, C. Adachi and T. Yasuda, High-Efficiency Blue Organic Light-Emitting Diodes Based on Thermally Activated Delayed Fluorescence from Phenoxaphosphine and Phenoxathiin Derivatives, *Adv. Mater.*, 2016, **28**, 4626–4631.



- 39 K. R. Naveen, H. Lee, R. Braveenth, D. Karthik, K. J. Yang, S. J. Hwang and J. H. Kwon, Achieving High Efficiency and Pure Blue Color in Hyperfluorescence Organic Light Emitting Diodes using Organo-Boron Based Emitters, *Adv. Funct. Mater.*, 2022, **32**, 2110356.
- 40 Y. Xu, P. Xu, D. Hu and Y. Ma, Recent progress in hot exciton materials for organic light-emitting diodes, *Chem. Soc. Rev.*, 2021, **50**, 1030–1069.
- 41 D. H. Ahn, S. W. Kim, H. Lee, I. J. Ko, D. Karthik, J. Y. Lee and J. H. Kwon, Highly efficient blue thermally activated delayed fluorescence emitters based on symmetrical and rigid oxygen-bridged boron acceptors, *Nat. Photonics*, 2019, **13**, 540–546.
- 42 U. Balijapalli, Y.-T. Lee, B. S. B. Karunathilaka, G. Tumen-Ulzii, M. Auffray, Y. Tsuchiya, H. Nakanotani and C. Adachi, Tetrabenzo[a,c]phenazine Backbone for Highly Efficient Orange–Red Thermally Activated Delayed Fluorescence with Completely Horizontal Molecular Orientation, *Angew. Chem., Int. Ed.*, 2021, **60**, 19364–19373.
- 43 Y.-K. Chen, J. Jayakumar, C.-L. Ko, W.-Y. Hung, T.-L. Wu and C.-H. Cheng, Increase the molecular length and donor strength to boost horizontal dipole orientation for high-efficiency OLEDs, *J. Mater. Chem. C*, 2022, **10**, 9241–9248.
- 44 Y. Fu, H. Liu, D. Yang, D. Ma, Z. Zhao and B. Z. Tang, Boosting external quantum efficiency to 38.6% of sky-blue delayed fluorescence molecules by optimizing horizontal dipole orientation, *Sci. Adv.*, 2021, **7**, eabj2504.
- 45 C. Qu, G. Xia, Y. Xu, Y. Zhu, J. Liang, H. Zhang, J. Wang, Z. Zhang and Y. Wang, Boron-containing D–A–A type TADF materials with tiny singlet–triplet energy splittings and high photoluminescence quantum yields for highly efficient OLEDs with low efficiency roll-offs, *J. Mater. Chem. C*, 2020, **8**, 3846–3854.
- 46 H. Jiang, P. Tao and W.-Y. Wong, Recent Advances in Triplet–Triplet Annihilation-Based Materials and Their Applications in Electroluminescence, *ACS Mater. Lett.*, 2023, **5**, 822–845.
- 47 Y. Im, M. Kim, Y. J. Cho, J.-A. Seo, K. S. Yook and J. Y. Lee, Molecular Design Strategy of Organic Thermally Activated Delayed Fluorescence Emitters, *Chem. Mater.*, 2017, **29**, 1946–1963.
- 48 H. Lee, D. Karthik, R. Lampande, J. H. Ryu and J. H. Kwon, Recent Advancement in Boron-Based Efficient and Pure Blue Thermally Activated Delayed Fluorescence Materials for Organic Light-Emitting Diodes, *Front. Chem.*, 2020, **8**, 373.
- 49 J. Han, Y. Chen, N. Li, Z. Huang and C. Yang, Versatile boron-based thermally activated delayed fluorescence materials for organic light-emitting diodes, *Aggregate*, 2022, **3**, e182.
- 50 H.-J. Tan, G.-X. Yang, Y.-L. Deng, C. Cao, J.-H. Tan, Z.-L. Zhu, W.-C. Chen, Y. Xiong, J.-X. Jian, C.-S. Lee and Q.-X. Tong, Deep-Blue OLEDs with Rec.2020 Blue Gamut Compliance and EQE Over 22% Achieved by Conformation Engineering, *Adv. Mater.*, 2022, **34**, 2200537.
- 51 I. S. Park, H. Min, J. U. Kim and T. Yasuda, Deep-Blue OLEDs Based on Organoboron–Phenazasiline-Hybrid Delayed Fluorescence Emitters Concurrently Achieving 30% External Quantum Efficiency and Small Efficiency Roll-Off, *Adv. Opt. Mater.*, 2021, **9**, 2101282.
- 52 A. Endo, M. Ogasawara, A. Takahashi, D. Yokoyama, Y. Kato and C. Adachi, Thermally Activated Delayed Fluorescence from Sn4 + –Porphyrin Complexes and Their Application to Organic Light Emitting Diodes — A Novel Mechanism for Electroluminescence, *Adv. Mater.*, 2009, **21**, 4802–4806.
- 53 K. Goushi, K. Yoshida, K. Sato and C. Adachi, Organic light-emitting diodes employing efficient reverse intersystem crossing for triplet-to-singlet state conversion, *Nat. Photonics*, 2012, **6**, 253–258.
- 54 M. Liu, R. Komatsu, X. Cai, K. Hotta, S. Sato, K. Liu, D. Chen, Y. Kato, H. Sasabe, S. Ohisa, Y. Suzuri, D. Yokoyama, S.-J. Su and J. Kido, Horizontally Orientated Sticklike Emitters: Enhancement of Intrinsic Out-Coupling Factor and Electroluminescence Performance, *Chem. Mater.*, 2017, **29**, 8630–8636.
- 55 H. J. Jang and J. Y. Lee, Key Factor Managing the Horizontal Emitting Dipole Orientation of a Thermally Activated Delayed Fluorescence Emitter in a Mixed Host, *ACS Appl. Mater. Interfaces*, 2022, **14**, 54907–54913.
- 56 X. Peng, W. Qiu, W. Li, M. Li, W. Xie, W. Li, J. Lin, J. Yang, X. Li and S.-J. Su, Synergetic Horizontal Dipole Orientation Induction for Highly Efficient and Spectral Stable Thermally Activated Delayed Fluorescence White Organic Light-Emitting Diodes, *Adv. Funct. Mater.*, 2022, **32**, 2203022.
- 57 R. Gómez-Bombarelli, J. Aguilera-Iparraguirre, T. D. Hirzel, D. Duvenaud, D. Maclaurin, M. A. Blood-Forsythe, H. S. Chae, M. Einzinger, D.-G. Ha, T. Wu, G. Markopoulos, S. Jeon, H. Kang, H. Miyazaki, M. Numata, S. Kim, W. Huang, S. I. Hong, M. Baldo, R. P. Adams and A. Aspuru-Guzik, Design of efficient molecular organic light-emitting diodes by a high-throughput virtual screening and experimental approach, *Nat. Mater.*, 2016, **15**, 1120–1127.
- 58 T. Hatakeyama, K. Shiren, K. Nakajima, S. Nomura, S. Nakatsuka, K. Kinoshita, J. Ni, Y. Ono and T. Ikuta, Ultrapure Blue Thermally Activated Delayed Fluorescence Molecules: Efficient HOMO–LUMO Separation by the Multiple Resonance Effect, *Adv. Mater.*, 2016, **28**, 2777–2781.
- 59 S. Madayanad Suresh, D. Hall, D. Beljonne, Y. Olivier and E. Zysman-Colman, Multiresonant Thermally Activated Delayed Fluorescence Emitters Based on Heteroatom-Doped Nanographenes: Recent Advances and Prospects for Organic Light-Emitting Diodes, *Adv. Funct. Mater.*, 2020, **30**, 1908677.
- 60 K. R. Naveen, P. Palanisamy, M. Y. Chae and J. H. Kwon, Multiresonant TADF materials: triggering the reverse intersystem crossing to alleviate the efficiency roll-off in OLEDs, *Chem. Commun.*, 2023, **59**, 3685–3702.
- 61 S. Hyun Lee, M. Young Chae, Y. Hun Jung, J. Hyeog Oh, H. Rin Kim, K. R. Naveen and J. H. Kwon, Enhanced triplet-triplet fusion for high efficiency and long lifetime of multi-resonant pure blue organic light emitting diodes, *J. Ind. Eng. Chem.*, 2023, **122**, 452–458.

- 62 R. K. Konidena, M. Yang and T. Yasuda, A  $\pi$ -extended tercarbazole-core multi-resonance delayed fluorescence emitter exhibiting efficient narrowband yellow electroluminescence, *Chem. Commun.*, 2023, **59**, 10251–10254, DOI: [10.1039/D3CC03241H](https://doi.org/10.1039/D3CC03241H).
- 63 K. R. Naveen, J. H. Oh, H. S. Lee and J. H. Kwon, Tailoring Extremely Narrow FWHM in Hypsochromic and Bathochromic Shift of Polycyclo-Heteraborin MR-TADF Materials for High-Performance OLEDs, *Angew. Chem., Int. Ed.*, 2023, **62**, e202306768.
- 64 D. Chen, W. Li, L. Gan, Z. Wang, M. Li and S.-J. Su, Non-noble-metal-based organic emitters for OLED applications, *Mater. Sci. Eng., R*, 2020, **142**, 100581.
- 65 J. Han, Y. Chen, N. Li, Z. Huang and C. Yang, Versatile boron-based thermally activated delayed fluorescence materials for organic light-emitting diodes, *Aggregate*, 2022, e182.
- 66 K. Shizu and H. Kaji, Comprehensive understanding of multiple resonance thermally activated delayed fluorescence through quantum chemistry calculations, *Commun. Chem.*, 2022, **5**, 53.
- 67 Y. Zhang, D. Zhang, J. Wei, X. Hong, Y. Lu, D. Hu, G. Li, Z. Liu, Y. Chen and L. Duan, Achieving Pure Green Electroluminescence with CIE<sub>y</sub> of 0.69 and EQE of 28.2% from an Aza-Fused Multi-Resonance Emitter, *Angew. Chem., Int. Ed.*, 2020, **59**, 17499–17503.
- 68 W. Xue, H. Yan, Y. He, L. Wu, X. Zhang, Y. Wu, J. Xu, J. He, C. Yan and H. Meng, Identifying the Molecular Origins of Green BN-TADF Material Degradation and Device Stability via in situ Raman Spectroscopy, *Chem. – Eur. J.*, 2022, **28**, e202201006.
- 69 K. Rayappa Naveen, K. Prabhu Cp, R. Braveenth and J. Hyuk Kwon, Molecular Design Strategy for Orange Red Thermally Activated Delayed Fluorescence Emitters in Organic Light-Emitting Diodes (OLEDs), *Chem. – Eur. J.*, 2022, **28**, e202103532.
- 70 C.-C. Yan, X.-D. Wang and L.-S. Liao, Thermally Activated Delayed Fluorescent Gain Materials: Harvesting Triplet Excitons for Lasing, *Adv. Sci.*, 2022, **9**, 2200525.
- 71 Y. Xu, C. Li, Z. Li, Q. Wang, X. Cai, J. Wei and Y. Wang, Constructing Charge-Transfer Excited States Based on Frontier Molecular Orbital Engineering: Narrowband Green Electroluminescence with High Color Purity and Efficiency, *Angew. Chem., Int. Ed.*, 2020, **59**, 17442–17446.
- 72 S. Oda, W. Kumano, T. Hama, R. Kawasumi, K. Yoshiura and T. Hatakeyama, Carbazole-Based DABNA Analogues as Highly Efficient Thermally Activated Delayed Fluorescence Materials for Narrowband Organic Light-Emitting Diodes, *Angew. Chem., Int. Ed.*, 2021, **60**, 2882–2886.
- 73 J. M. Ha, S. H. Hur, A. Pathak, J.-E. Jeong and H. Y. Woo, Recent advances in organic luminescent materials with narrowband emission, *NPG Asia Mater.*, 2021, **13**, 53.
- 74 Y. Liu, X. Xiao, Y. Ran, Z. Bin and J. You, Molecular design of thermally activated delayed fluorescent emitters for narrowband orange-red OLEDs boosted by a cyano-functionalization strategy, *Chem. Sci.*, 2021, **12**, 9408–9412.
- 75 K. R. Naveen, S. J. Hwang, H. Lee and J. H. Kwon, Narrow Band Red Emission Fluorophore with Reasonable Multiple Resonance Effect, *Adv. Electron. Mater.*, 2022, **8**, 2101114.
- 76 S. M. Cho, K. M. Youn, H. I. Yang, S. H. Lee, K. R. Naveen, D. Karthik, H. Jeong and J. H. Kwon, Anthracene-dibenzofuran based electron transport type hosts for long lifetime multiple resonance pure blue OLEDs, *Org. Electron.*, 2022, **105**, 106501.
- 77 Y. Xu, Z. Cheng, Z. Li, B. Liang, J. Wang, J. Wei, Z. Zhang and Y. Wang, Molecular-Structure and Device-Configuration Optimizations toward Highly Efficient Green Electroluminescence with Narrowband Emission and High Color Purity, *Adv. Opt. Mater.*, 2020, **8**, 1902142.
- 78 Y. Zhang, D. Zhang, J. Wei, Z. Liu, Y. Lu and L. Duan, Multi-Resonance Induced Thermally Activated Delayed Fluorophores for Narrowband Green OLEDs, *Angew. Chem., Int. Ed.*, 2019, **58**, 16912–16917.
- 79 D. Li, H. Zhang and Y. Wang, Four-coordinate organoboron compounds for organic light-emitting diodes (OLEDs), *Chem. Soc. Rev.*, 2013, **42**, 8416–8433.
- 80 K. R. Naveen, H. Lee, R. Braveenth, K. J. Yang, S. J. Hwang and J. H. Kwon, Deep blue diboron embedded multi-resonance thermally activated delayed fluorescence emitters for narrowband organic light emitting diodes, *Chem. Eng. J.*, 2022, **432**, 134381.
- 81 K. R. Naveen, H. Lee, L. H. Seung, Y. H. Jung, C. P. Keshavananda Prabhu, S. Muruganatham and J. H. Kwon, Modular design for constructing narrowband deep-blue multi-resonant thermally activated delayed fluorescent emitters for efficient organic light emitting diodes, *Chem. Eng. J.*, 2023, **451**, 138498.
- 82 D. Karthik, Y. H. Jung, H. Lee, S. Hwang, B.-M. Seo, J.-Y. Kim, C. W. Han and J. H. Kwon, Acceptor–Donor–Acceptor-Type Orange–Red Thermally Activated Delayed Fluorescence Materials Realizing External Quantum Efficiency Over 30% with Low Efficiency Roll-Off, *Adv. Mater.*, 2021, **33**, 2007724.
- 83 B. Li, H. Nomura, H. Miyazaki, Q. Zhang, K. Yoshida, Y. Suzuma, A. Orita, J. Otera and C. Adachi, Dicarbazolyldicyanobenzenes as Thermally Activated Delayed Fluorescence Emitters: Effect of Substitution Position on Photoluminescent and Electroluminescent Properties, *Chem. Lett.*, 2013, **43**, 319–321.
- 84 Z. Zhang, E. Crovini, P. L. dos Santos, B. A. Naqvi, D. B. Cordes, A. M. Z. Slawin, P. Sahay, W. Brütting, I. D. W. Samuel, S. Bräse and E. Zysman-Colman, Efficient Sky-Blue Organic Light-Emitting Diodes Using a Highly Horizontally Oriented Thermally Activated Delayed Fluorescence Emitter, *Adv. Opt. Mater.*, 2020, **8**, 2001354.
- 85 G. Meng, H. Dai, Q. Wang, J. Zhou, T. Fan, X. Zeng, X. Wang, Y. Zhang, D. Yang, D. Ma, D. Zhang and L. Duan, High-efficiency and stable short-delayed fluorescence emitters with hybrid long- and short-range charge-transfer excitations, *Nat. Commun.*, 2023, **14**, 2394.
- 86 K. R. Naveen, R. K. Konidena and P. Keerthika, Neoteric Advances in Oxygen Bridged Triaryl Boron-based Delayed Fluorescent Materials for Organic Light Emitting Diodes, *Chem. Rec.*, 2023, e202300208.
- 87 J. Lee, K. Shizu, H. Tanaka, H. Nakanotani, T. Yasuda, H. Kaji and C. Adachi, Controlled emission colors and

- singlet–triplet energy gaps of dihydrophenazine-based thermally activated delayed fluorescence emitters, *J. Mater. Chem. C*, 2015, **3**, 2175–2181.
- 88 T. Zhao, S. Jiang, X.-D. Tao, M. Yang, L. Meng, X.-L. Chen and C.-Z. Lu, Dihydrophenazine-derived thermally activated delayed fluorescence emitters for highly efficient orange and red organic light-emitting diodes, *Dyes Pigm.*, 2023, **211**, 111065.
- 89 J.-X. Hu, S. Jiang, D.-H. Zhang, T. Zhao, F.-L. Lin, L. Meng, X.-L. Chen and C.-Z. Lu, Rational Design of Highly Efficient Orange-Red/Red Thermally Activated Delayed Fluorescence Emitters with Submicrosecond Emission Lifetimes, *Adv. Sci.*, 2023, **10**, 2300808.
- 90 Y.-H. He, F.-M. Xie, K. Zhang, D. Yang, Y. Shen, H.-Z. Li, D. Ma, Y.-Q. Li and J.-X. Tang, Acceptor–Donor–Acceptor-Configured Delayed Fluorescence Emitters for Efficient Orange-Red and White Devices with Low Roll-off, *Adv. Funct. Mater.*, 2023, 2304006.
- 91 F.-M. Xie, H.-Z. Li, K. Zhang, Y. Shen, X. Zhao, Y.-Q. Li and J.-X. Tang, A Dislocated Twin-Locking Acceptor–Donor–Acceptor Configuration for Efficient Delayed Fluorescence with Multiple Through-Space Charge Transfer, *Angew. Chem., Int. Ed.*, 2022, **61**, e202213823.
- 92 Y. Ye, Y. He and X. Xiu, Manipulating Ultra-High Definition Video Traffic, *IEEE MultiMedia*, 2015, **22**, 73–81.
- 93 X. Zeng, Y.-H. Huang, S. Gong, P. Li, W.-K. Lee, X. Xiao, Y. Zhang, C. Zhong, C.-C. Wu and C. Yang, An unsymmetrical thermally activated delayed fluorescence emitter enables orange-red electroluminescence with 31.7% external quantum efficiency, *Mater. Horiz.*, 2021, **8**, 2286–2292.
- 94 H. Liu, Q. Bai, W. Li, Y. Guo, L. Yao, Y. Gao, J. Li, P. Lu, B. Yang and Y. Ma, Efficient deep-blue non-doped organic light-emitting diode with improved roll-off of efficiency based on hybrid local and charge-transfer excited state, *RSC Adv.*, 2016, **6**, 70085–70090.
- 95 B. Liu, Z.-L. Zhu, J.-W. Zhao, D. He, Z.-Y. Wang, C.-Y. Luo, Q.-X. Tong, C.-S. Lee and S.-L. Tao, Ternary Acceptor–Donor–Acceptor Asymmetrical Phenanthroimidazole Molecule for Highly Efficient Near-Ultraviolet Electroluminescence with External Quantum Efficiency (EQE) > 4%, *Chem. – Eur. J.*, 2018, **24**, 15566–15571.
- 96 W. Yuan, H. Yang, M. Zhang, D. Hu, S. Wan, Z. Li, C. Shi, N. Sun, Y. Tao and W. Huang, Molecular engineering on all ortho-linked carbazole/oxadiazole hybrids toward highly-efficient thermally activated delayed fluorescence materials in OLEDs, *Chin. Chem. Lett.*, 2019, **30**, 1955–1958.
- 97 S. M. Suresh, L. Zhang, T. Matulaitis, D. Hall, C. Si, G. Ricci, A. M. Z. Slawin, S. Warriner, D. Beljonne, Y. Olivier, I. D. W. Samuel and E. Zysman-Colman, Judicious Heteroatom Doping Produces High-Performance Deep-Blue/Near-UV Multiresonant Thermally Activated Delayed Fluorescence OLEDs, *Adv. Mater.*, 2023, **35**, 2300997.
- 98 C. Jiang, J. Miao, D. Zhang, Z. Wen, C. Yang and K. Li, Acceptor–Donor–Acceptor  $\pi$ -Stacking Boosts Intramolecular Through-Space Charge Transfer towards Efficient Red TADF and High-Performance OLEDs, *Research*, 2022, 9892802.